A compositional investigation for bandgap engineering of wide bandgap triple cation perovskite

Jacopo Sala[†,‡,#], Maryamsadat Heydarian[†,#], Stijn Lammar[†,‡], Yaser Abdulraheem[♦], Tom Aernouts[†], Afshin Hadipour[*,†] and Jef Poortmans[†,‡]

† Thin-Film PV, imec – partner in EnergyVille and Solliance, Thor Park 8320, 3600 Genk, Belgium

‡ Department of Electrical Engineering, KU Leuven, 3000 Leuven, Belgium

♦ Department of Electrical Engineering, Kuwait University, P.O. Box 5969, Safat 13060 13060 Kuwait

AUTHOR INFORMATION

# J. Sala and M. Heydarian contributed equally to this work.

Corresponding Author

* E-mail: afshin.hadipour@imec.be

Abstract: Perovskite solar cells have shown their potential for multijunction applications due to their tunable bandgap. Here a compositional investigation on 3C perovskites is presented to map the bandgap and electrical output of different perovskites. The research focuses on wide bandgap perovskites ranging from 1.6 eV to 1.76 eV, which are the ideal choice for silicon-perovskite or all-perovskite 2-terminal tandems. The bandgap is changed via the most common X-site substitution of iodine with bromine and via cation substitution, with various concentrations of cesium, methylammonium (MA) and formamidinium (FA). As a result, it is seen that cation engineering is a viable solution to fine-tune the bandgap and to prevent photo-induced segregation of the perovskite. The most promising compositions with 1.67eV showed a champion efficiency of 18.25% in a single-junction configuration.
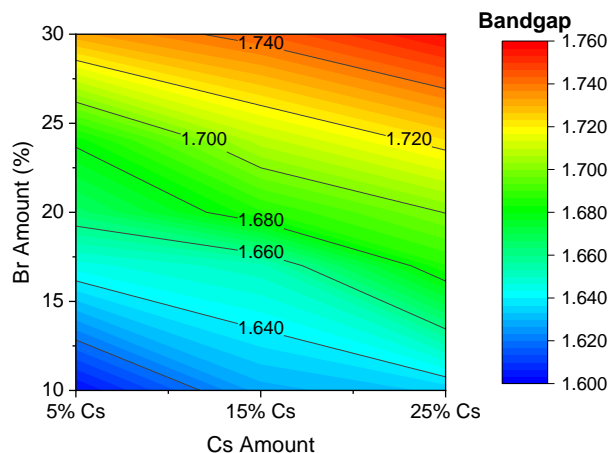
Figure 1: Graphical abstract, Bandgap variation based on Cs, Br contents in 3C perovskite

Organo-metal halide perovskites have already demonstrated their potential as power generators with efficiencies rapidly increasing from 3.8% to 25.5% at research scale in just a decade[1]. This establishes perovskite solar cells as the fastest growing photovoltaic technology at research scale to date and it is now considered as a realistic industrial alternative for low-cost electricity

generation[2]. Perovskites for PV applications are of the form ABX_3 in which the most common components are MA, Cs, FA at the A-site, Pb at the B-site and I, Br, Cl at the X site. This perovskite composition's flexibility is ideal to produce absorbing semiconductor materials with a variable bandgap ranging from 1.47eV for $FAPbI_3$[3] to more than 3.06eV when chlorine is used with cesium to form $CsPbCl_3$[4]. The adoption of different bandgaps is a strong advantage of this technology as it can tune its absorption edge to optimize the photocurrent generation in multijunction solar cells maximizing their power conversion efficiency. In fact, in just a few years, perovskite-based tandems have shown remarkable progress and almost reached the ambitious target of 30% efficiency on silicon and more than 24.2% on CIGS[1]. However, to properly tune the perovskite composition it is necessary to balance the A-site cations and the X-site halides. The most common way to increase the bandgap of metal-organic halide perovskite is to substitute iodine with other halides such as bromine or chlorine[5–7]. In the case of $MAPbI_3$ a full substitution with Br and Cl increases the bandgap from 1.55 eV, up to 2.24 eV and 2.97 eV respectively[8]. However, the A-site cations can also contribute effectively to tune the bandgap with $FAPbI_3$ and $CsPbI_3$ bandgaps being respectively 1.47 eV[3] and 1.77 eV.[4] In fact, as explained by K. Bush et al.[9] and by Prasanna et al.[10], smaller cations such as Cs, can tilt the BX_6 octahedra when in the tetragonal structure, reducing the X−B−X bond angle and increasing the bandgap.

So far, the research community has been challenged to find phase-stable wide bandgap compounds as they tend to segregate under illumination. A first understanding of the underlying mechanisms was proposed by Hoke et al., who identified the formation of Iodine-rich and Bromine-rich clusters under illumination[11]. Since then, the research community concentrated on tuning the Br/I ratio at the X site to target a desired bandgap and different approaches have been proposed to stabilize the composition. For example, solvent engineering and the inclusion of a

multi-cation system with a balanced ratio of Cs and FA permitted Jaysankar et al. to achieve a 1.72eV stable structure with improved photo-stability and a 4T efficiency of 27.1%[5]. Following this trend, 3C and 4C perovskites were used to create high efficiency wide bandgap perovskites reaching multijunction power conversion efficiencies higher than 29.15%[12].

Moreover, the current state of the art perovskite records have mostly exploited antisolvents to rapidly achieve a supersaturation status to quench the perovskite solution and obtain bigger grain sizes via a fast nucleation of the crystals for enhanced electronic properties[13]. However, the standard solvent mixture of dimethylformamide (DMF) and dimethyl sulfoxide (DMSO) has a limited window for processing the perovskite layer for devices with larger areas by using tools such as a slot die coater[14], where the perovskite is quenched via gas-assisted techniques instead of antisolvents. On the other hand, N-Methyl-2-pyrrolidone (NMP) shows more promising results than DMSO for perovskite deposited via an up-scalable approach and gas-assisted quenching techniques[15–17]. Therefore, a solution mixture of DMF/NMP is used in this research and the gas-assisted quenching route[18,19] is chosen to better reproduce up-scalable conditions.

In this work, we explore the bandgap variations in relation to cations and halides for a triple cation perovskite $Cs_x(MA_zFA_{1-z})_{1-x}Pb(I_{1-y}Br_y)_3$. The values x, y and z are respectively expressed as $\%_{Cs}$, $\%_{Br}$ and $\%_{MA}$. The initial focus of this research is on the concentration ratio of Cs over (MA, FA), or $\%_{Cs}$ at the A-site and on $\%_{Br}$ at the X-site. Instead, the $\%_{MA}$ is initially maintained constant at 1:4 to focus on the effects of bandgap variations due to the inclusion of cesium in the perovskite composition and will be discussed at a later moment. The compositional analysis is made in 3 different days. Each time, a fixed concentration of cesium (5%, 15% and 25%) is used while the bromine content varies from 10% to 17%, 20%, 24% and 30%. The compositions are

selected in order to be comparable with the recognized community standard antisolvent recipes $Cs_{0.05}(MA_{0.17}FA_{0.83})_{0.95}Pb(I_{0.83}Br_{0.17})_3$[20] and $Cs_{0.05}(MA_{0.24}FA_{0.76})_{0.95}Pb(I_{0.76}Br_{0.24})_3$[21].

Figure 2 show how the bandgap increases in a linear relation to the Br concentration. The bandgap value is here measured as the inflection point of the External Quantum Efficiency (EQE) band tail, as explained by Krückemeier et al.[22] and used by Jiang et al.[23]. Based on the acquired quantum efficiency reported in **Figure 4**, it is seen that the bandgap ranges from 1.6eV for 5%$_{Cs}$ - 10%$_{Br}$ to a 1.76 eV for 25%$_{Cs}$ when 30%$_{Br}$ is used, as reported in **Figure 2Error! Reference source not found.**. Similarly, when Cs is varied the bandgap generates a similar trend, as values with a specific Br amount appear to be equally spaced in the y-axis. A linear regression of the data separated by cesium content shows a slope of 6.32 ± 0.37 meV/%$_{Br}$, 5.98 ± 0.54 meV/%$_{Br}$, 6.08 ± 0.28 meV/%$_{Br}$ for the compositions with 5%$_{Cs}$, 15%$_{Cs}$, 25%$_{Cs}$, respectively. This is in agreement with the value of 5.7 ± 0.2 meV/%$_{Br}$ previously reported for a Cs, FA double cation investigation[9].
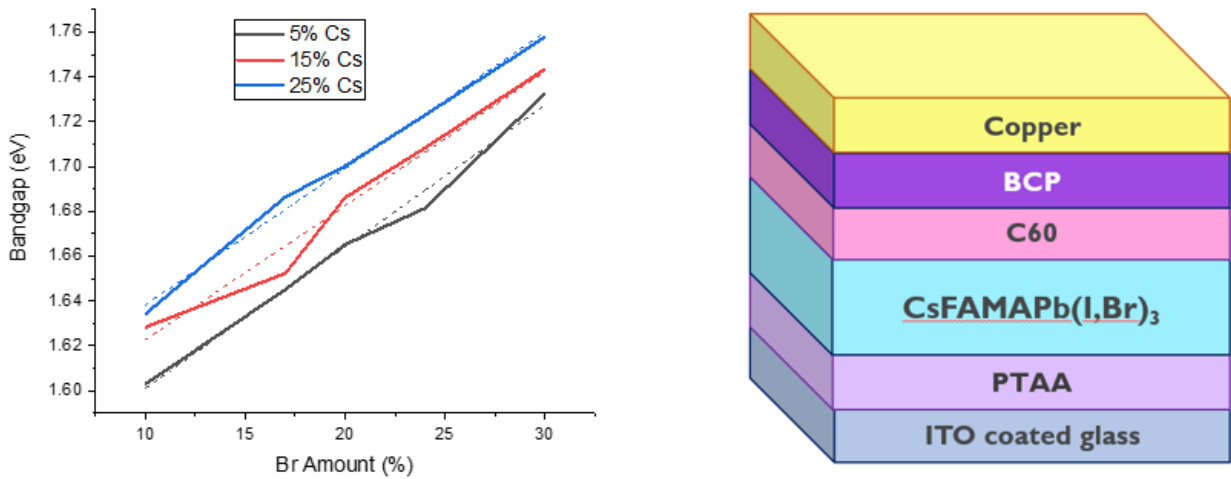
Figure 2: Bandgap variation for different Bromine concentrations (left), ITO/PTAA /Perovskite/C60/BCP/Cu PIN structure (right)

In addition, to assess the electronic quality of the solar cells, full devices were created with a PIN structure composed of ITO/PTAA/Perovskite/C60/BCP/Cu (**Figure 2**: right) and their electrical JV parameters were measured. As expected from the analysis on the bandgap, the devices showed a reduction in J_{sc} and an increase in V_{oc} in accordance with the increase in bromine content. As reported in **Table S1** and shown in **Figure 3**, the short circuit current drops 3.2 mA/cm^2 for bromine content between 10%$_{Br}$ and 30%$_{Br}$ for both 15%$_{Cs}$ and 25%$_{Cs}$, respectively. Instead, a steeper loss is shown for 5%$_{Cs}$ as 24%$_{Br}$ already loses 3.2 mA/cm^2 and 30%$_{Br}$ loses 5.8 mA/cm^2. On the other hand, the V_{oc} increases with a ratio V_{oc} to bandgap of 0.5 V/eV for each fixed amount of %$_{Cs}$, even though a value closer to 1 V/eV would be expected from theoretical calculations[22,24].
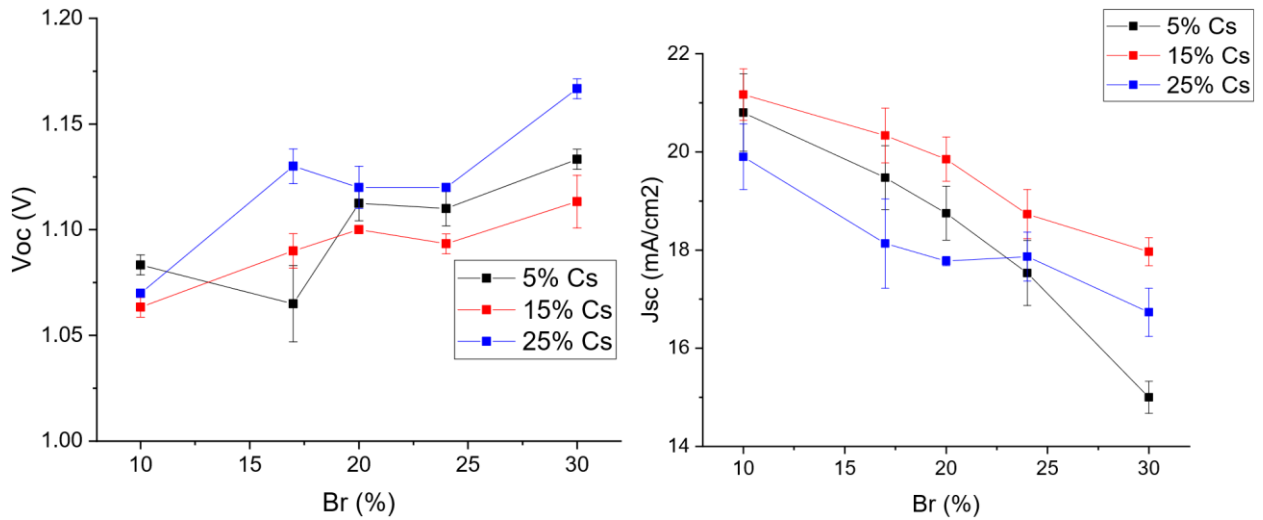

Figure 3: Voc (right) and Jsc (left) for various Cs and Br compositions

Moreover, these electrical results are checked in comparison with EQE measurements. The graphs clearly show the band-edge shifting towards lower wavelengths for compositions with increased Br content, as shown in **Figure 4**. Besides, the photon to current conversion efficiency is on average maintained between 85 - 90% in the 400 – 670 nm range, which shows good electronic properties in all the cases. Note here that the different shapes for wavelengths shorter

than 400 nm are due to variation of thicknesses of PTAA and its absorption for different PIN devices as confirmed by the optical simulation reported in **Figure S1**.

Table 1: Integrated Jsc from EQE in mA/cm^2

Cs\Br	10	17	20	24	30
5	21.87	20.46	19.93	20.25	18.09
15	20.77	19.92	18.92	18.85	18.12
25	20.81	20.37	19.23	19.47	18.64
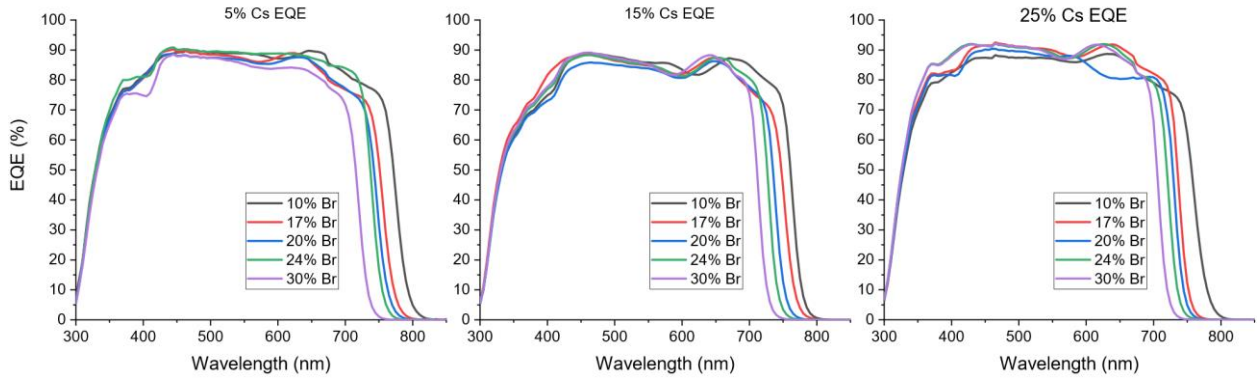
Figure 4: External quantum efficiency graphs for 5%Cs (left), 15%Cs (center), 25%Cs (right)
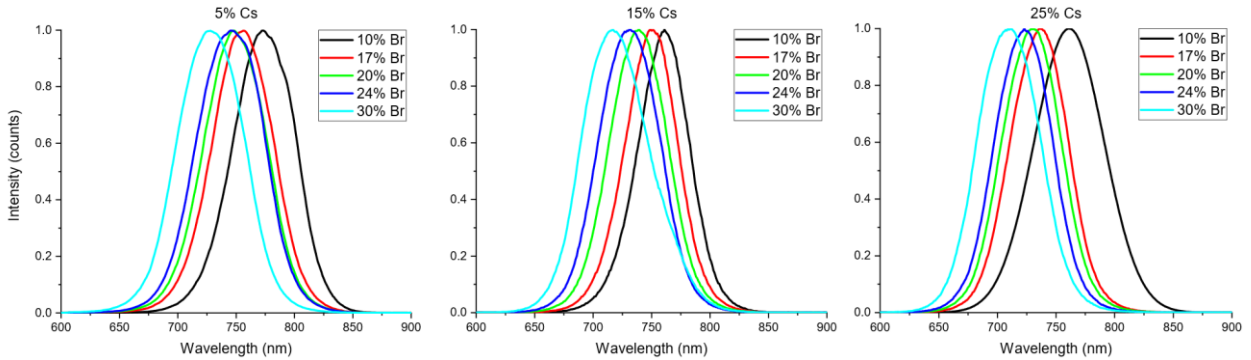
Figure 5: Normalized photoluminescence peaks for the previously presented compositions. 5%Cs (left), 15%Cs (center), 25%Cs (right)

From this analysis it is certain that the introduction of cesium is beneficial to increase the bandgap, as it is demonstrated by the blue shift of the PL peaks and EQE absorption edges in **Figure 4** and **Figure 5**. Moreover, similar charge extraction efficiencies for the additional introduction of the cation can be confirmed by the high EQE. Therefore, in order to correctly evaluate the beneficial inclusion of Cs in terms of J_{sc}, a separate experiment with a fixed $20\%_{Br}$ content and varying cesium amount was performed. The choice of $20\%_{Br}$ relates to the interest towards bandgaps in the range of 1.65eV – 1.7eV for possible tandem applications on silicon devices.

**Table 2:** JV characteristics of different Cs concentrations, with a fixed Br

Br %	Cs %	Bandgap (eV)	Jsc (mA/cm2)	Voc (V)	FF (%)	PCE (%)
20% Br	5 %	1.66 eV	17.7 ± 1.0	1.07 ± 0.02	72.05 ± 1.11	13.66 ± 0.75
	15 %	1.68 eV	18.0 ± 0.7	1.08 ± 0.02	73.13 ± 1.36	14.21 ± 0.47
	25 %	1.70 eV	17.8 ± 0.7	1.14 ± 0.02	71.28 ± 1.00	14.46 ± 0.42

A first look at the electrical characterization shows immediately a clear impact of Cs inclusion on the value of V_{oc} as it increases more than the increase in bandgap. On the other hand, the short circuit current density of the three samples is almost unchanged, in contradiction to what would have been expected by the increase in bandgap. This combined effect is also reflected in a gradual increase in efficiency. The results are confirmed as well via EQE measurements where the J_{sc} is 19.19 mA/cm^2, 18.94 mA/cm^2 and 18.98 mA/cm^2 for $25\%_{Cs}$, $15\%_{Cs}$, $5\%_{Cs}$, respectively. Besides the correspondence, that may not be strictly appropriate for the effects of the optical interference in the $25\%_{Cs}$ case, it is possible to notice a trending increase between 300 nm to 500 nm, which

shows better charges extraction. In addition, scanning electron microscope (SEM) top view images show bigger grains with increased amount of Cs, which is usually associated with improved conductivity[25] (see **Figure S2**) .

To further understand the effects introduced by Cs in this composition, the crystallographic structure was investigated via X-Ray Diffraction (XRD) and the refractive index and extinction coefficients were measured via ellipsometry. The XRD output presents shifted perovskite peaks such that the main signal referring to a (001) orientation moves from 14.04° to 14.08° and 14.18° for 25%$_{Cs}$, 15%$_{Cs}$, 5%$_{Cs}$, respectively. Similarly, the (002) peak also moves from 28.44° to 28.5° and 28.62° for 25%$_{Cs}$, 15%$_{Cs}$, 5%$_{Cs}$, as shown in **Figure 7**. This follows the insertion of the smaller cation Cs (167 pm) with FA (253 pm) and MA (217 pm) as the smaller radius contracts the perovskite lattice and increases the energy level distance in the Pb atoms[26]. Moreover, the FWHM also reduces from 0.5° to 0.46° and 0.35°.
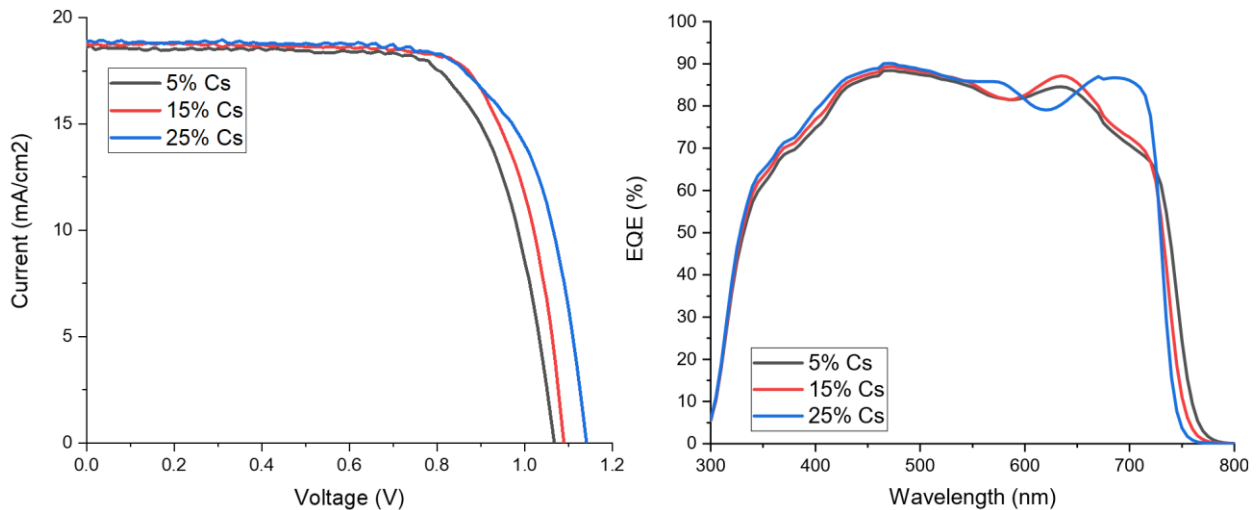
Figure 6: JV and EQE graphs for increased Cs amount

The ellipsometry results show a shift in the absorption edge related to the photoluminescence peaks shift towards lower wavelengths as expected. Moreover, the extinction coefficient (k-value)

does not reduce with increased amounts of Cs in the region below 700 nm as previously reported

by M. Saliba et Al.[20], meaning that the absorption coefficients is not affected by this change.
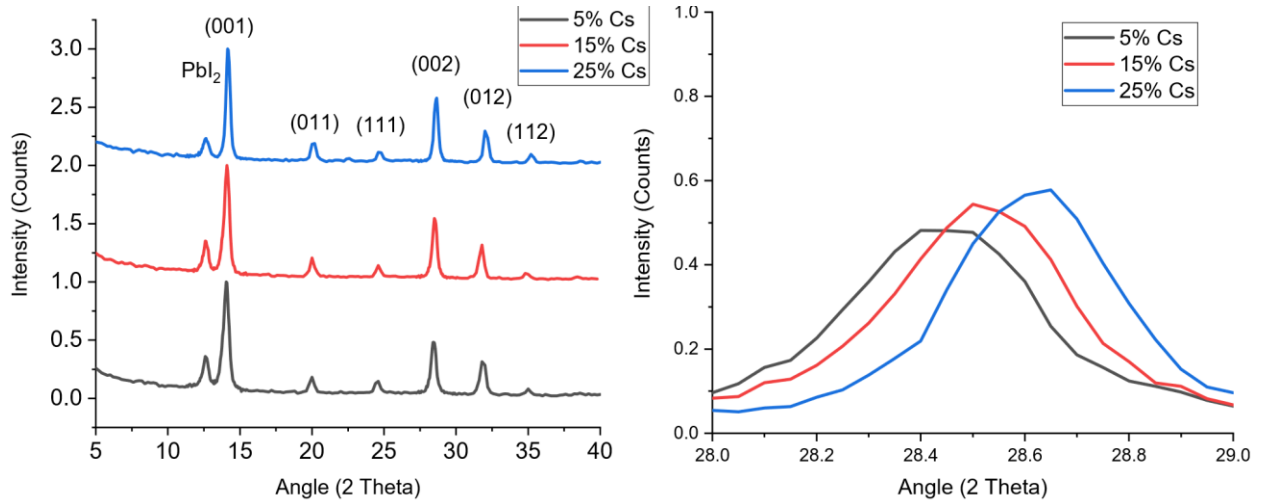
Figure 7: XRD measurements for 5%, 15%, 25%Cs (Left), a focused look at the (002) peak for
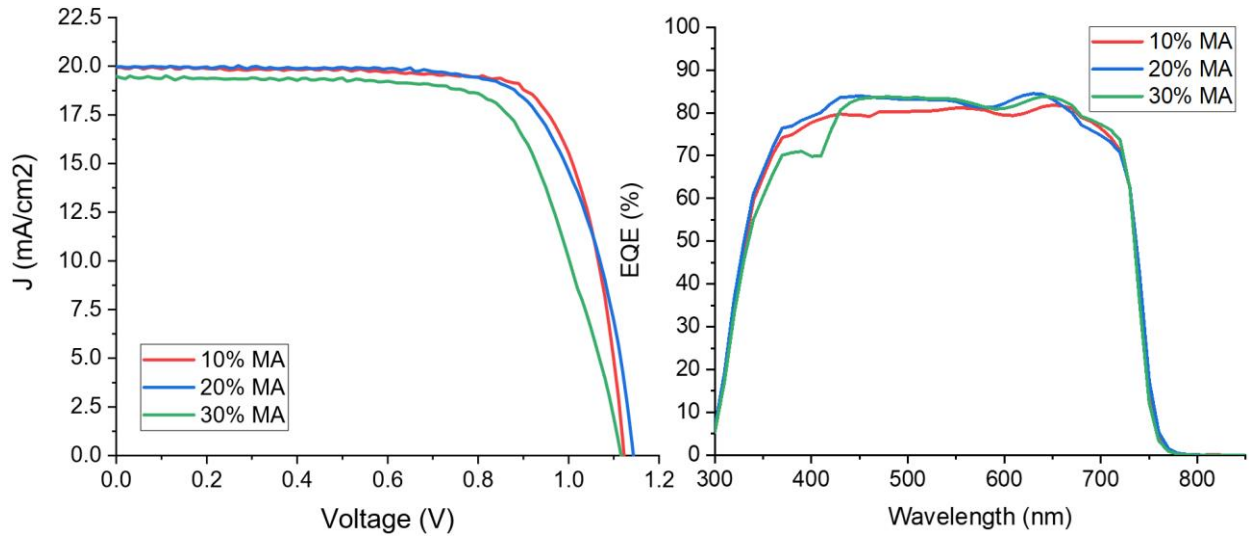
perovskites
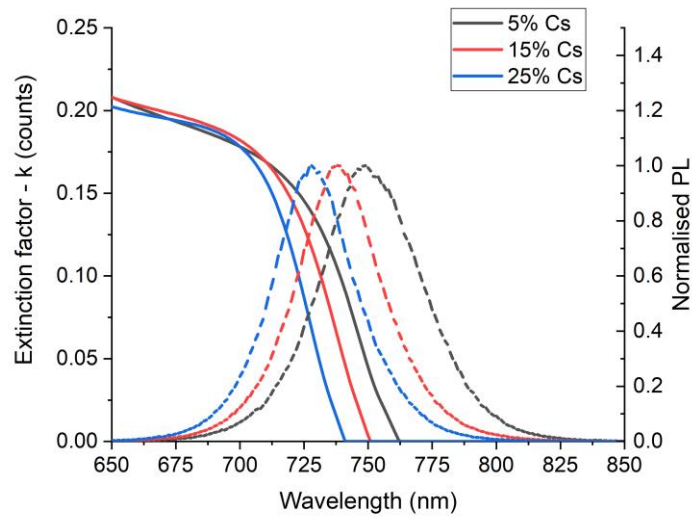
Figure 8: Extinction coefficient (full lines) and normalized photoluminescence peaks (dashed

lines)

Continuing with the investigation on the effects of various cation compositions, FA and MA ratios are considered next. The introduction of additional amounts of MA over FA is expected to generate similar trends to Cs over the perovskite bandgap, since MA has a smaller structure than FA. However, the bigger radius of MA in respects to Cs is expected to have a reduced impact. In order to assess the possible effects of MA, its concentration over FA is tested with 15% cesium and 20% bromine.

Table 3: JV electrical characterization for MA, FA ratio variation.

MA content	Bandgap (eV)	EQE Jsc (mA/cm2)	Jsc (mA/cm2)	Voc (V)	FF (%)	Eff (%)
10% MA	1.66	19.58	18.9 ± 0.5	1.11 ± 0.00	76.49 ± 0.42	16.0 ± 0.3
20% MA	1.67	20.01	19.9 ± 0.1	1.14 ± 0.01	71.77 ± 0.89	16.2 ± 0.3
30% MA	1.68	19.8	18.5 ± 0.7	1.12 ± 0.00	69.09 ± 0.36	14.4 ± 0.5

The JV results show that MA does not substantially alter the Voc, while an excess of MA induces a lower FF. A similar conclusion was also previously reported by Tan et Al.[27] for a maximum inclusion of 15% MA. In their work, it was also proposed that the inclusion of a dipolar cation such as MA can reduce defects such as Pb vacancies, which leads to a reduced amount of deep trap states leading to longer carrier lifetimes. Furthermore, MA seems to slightly benefit J_{sc} as shown by the 400nm – 700nm range of the EQE, which also shows a small shift in the absorption edge and photovoltaic bandgap, further confirmed by photoluminescence measurements.

Figure 9: JV (left) and EQE (right) measurements for different MA/FA ratio.

To sum up what was discussed so far, it is possible to vary the composition of a 3C perovskite to obtain the desired bandgap, while preserving high performance devices with relatively large PCEs. Not only that, but the introduction of different cation concentrations can also be beneficial in fine-tuning the bandgap.

As from the proposed perovskites, the $15\%_{Cs}$, $20\%_{Br}$ option seems to be an optimal choice for tandem applications based on silicon technology, with a suitable bandgap of 1.67eV and a J_{sc} of almost 20 mA/cm^2. In fact, such composition can achieve current matching while maximizing the open circuit voltage of a two-terminal multijunction device. As the whole analysis was performed with perovskite solutions' concentrations of 1 M, increased concentrations are used to achieve higher currents. With the selected composition, an experiment was performed with concentrations of 1 M, 1.1 M, 1.2 M, 1.3 M and 1.4 M.

The J_{sc} already increases by 1 mA/cm^2 from 1 M to 1.1 M and continuously increases up to 20.1mA/cm^2 for 1.4 M. The V_{oc} at the same time does not change, which demonstrates a good bulk

conductivity of charges and a limited defect induced losses in the bulk. With this increase it has been possible to achieve a champion device with a J_{sc} of 20.6 mA/cm2, a V_{oc} of 1.13 V and a FF of 78.35% giving an overall power conversion efficiency of 18.25%.

Table 4: JV electrical characterization with increased Molarity

Perovskite concentration	Thickness (nm)	Jsc (mA/cm2)	Voc (V)	Fill Factor (%)	Efficiency (%)	Champ. Eff. (%)
1.4 M	626.9 ± 3.6	20.1 ± 0.6	1.13 ± 0.01	78.11 ± 0.23	17.7 ± 0.7	18.25
1.3 M	501.5 ± 8.8	19.8 ± 0.8	1.13 ± 0.01	77.18 ± 1.34	17.3 ± 0.6	17.69
1.2 M	442.1 ± 0.8	19.8 ± 0.4	1.13 ± 0.00	77.87 ± 0.64	17.4 ± 0.5	17.90
1.1 M	419.0 ± 1.0	19.3 ± 0.6	1.13 ± 0.01	77.92 ± 0.49	17.0 ± 0.5	17.33
1.0 M	392.2 ± 0.5	18.5 ± 0.7	1.14 ± 0.01	78.27 ± 0.27	16.4 ± 0.4	16.01
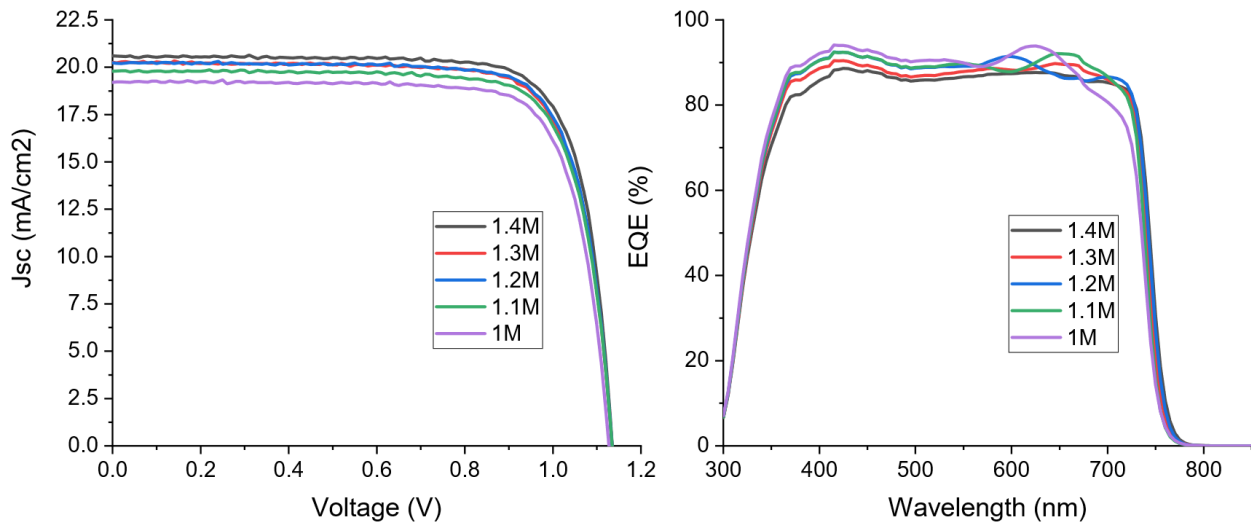
Figure 10: JV (left) and EQE (right) curves of champion cells for increased solution concentration

In conclusion, a bandgap engineering investigation on wide bandgap 3C perovskites suitable for silicon based multijunction applications produced via upscalable and industrially compatible

techniques is here presented. Even though Br remains a strong element in bandgap tuning for perovskite solar cells, this work shows that Cs and other cations are essential to achieve phase-stable wide bandgap perovskites and to fine-tune the absorption edge. Moreover, these absorbing layers performed well even with more concentrated solutions and increased thicknesses, which permits a proper adjustment of the final thickness.

ASSOCIATED CONTENT

Supporting Information. Detailed device fabrication and characterization with additional plots

AUTHOR INFORMATION

Corresponding author: afshin.hadipour@imec.be

Notes

"The authors declare no competing financial interest."

REFERENCES

(1)   NREL. Best Research Cell Efficiencies. 2020.

(2)   IEA. *World Energy Outlook 2020*; Paris.

(3)   Yang, W. S.; Noh, J. H.; Jeon, N. J.; Kim, Y. C.; Ryu, S.; Seo, J.; Seok, S. Il. High-Performance Photovoltaic Perovskite Layers Fabricated through Intramolecular Exchange. *Science (80-.).* **2015**, *348* (6240), 1234–1237. https://doi.org/10.1126/science.aaa9272.

(4)   Saliba, M.; Correa-Baena, J. P.; Grätzel, M.; Hagfeldt, A.; Abate, A. Perovskite Solar Cells: From the Atomic Level to Film Quality and Device Performance. *Angew. Chemie - Int. Ed.* **2018**, *57* (10), 2554–2569. https://doi.org/10.1002/anie.201703226.

(5)   Jaysankar, M.; Raul, B. A. L. L.; Bastos, J.; Burgess, C.; Weijtens, C.; Creatore, M.; Aernouts, T.; Kuang, Y.; Gehlhaar, R.; Hadipour, A.; Poortmans, J.; Raul, B. A. L. L.; Bastos, J.; Aernouts, T.; Jaysankar, M.; Burgess, C.; Hadipour, A.; Gehlhaar, R.; Kuang, Y.; Creatore, M.; Raul, B. A. L. L.; Bastos, J.; Burgess, C.; Weijtens, C.; Creatore, M.; Aernouts, T.; Kuang, Y.; Gehlhaar, R.; Hadipour, A.; Poortmans, J.; Raul, B. A. L. L.; Bastos, J.; Aernouts, T.; Jaysankar, M.; Burgess, C.; Hadipour, A.; Gehlhaar, R.; Kuang, Y.; Creatore, M. Minimizing Voltage Loss in Wide-Bandgap Perovskites for Tandem Solar Cells. *ACS Energy Lett.* **2019**, *4* (1), 259–264. https://doi.org/10.1021/acsenergylett.8b02179.

(6)   Xu, J.; Boyd, C. C.; Yu, Z. J.; Palmstrom, A. F.; Witter, D. J.; Larson, B. W.; France, R. M.; Werner, J.; Harvey, S. P.; Wolf, E. J.; Weigand, W.; Manzoor, S.; Van Hest, M. F. A. M.; Berry, J. J.; Luther, J. M.; Holman, Z. C.; McGehee, M. D. Triple-Halide Wide-Band Gap Perovskites with Suppressed Phase Segregation for Efficient Tandems. *Science (80-.).* **2020**, *367* (6482), 1097–1104. https://doi.org/10.1126/science.aaz4639.

(7)   Gharibzadeh, S.; Abdollahi Nejand, B.; Jakoby, M.; Abzieher, T.; Hauschild, D.; Moghadamzadeh, S.; Schwenzer, J. A.; Brenner, P.; Schmager, R.; Haghighirad, A. A.; Weinhardt, L.; Lemmer, U.; Richards, B. S.; Howard, I. A.; Paetzold, U. W. Record Open-Circuit Voltage Wide-Bandgap Perovskite Solar Cells Utilizing 2D/3D Perovskite Heterostructure. *Adv. Energy Mater.* **2019**, *1803699*, 1–10. https://doi.org/10.1002/aenm.201803699.

(8)   Leguy, A. M. A.; Azarhoosh, P.; Alonso, M. I.; Campoy-Quiles, M.; Weber, O. J.; Yao, J.; Bryant, D.; Weller, M. T.; Nelson, J.; Walsh, A.; Van Schilfgaarde, M.; Barnes, P. R. F. Experimental and Theoretical Optical Properties of Methylammonium Lead Halide Perovskites. *Nanoscale* **2016**, *8* (12), 6317–6327. https://doi.org/10.1039/c5nr05435d.

(9)   Bush, K. A.; Frohna, K.; Prasanna, R.; Beal, R. E.; Leijtens, T.; Swifter, S. A.; McGehee, M. D. Compositional Engineering for Efficient Wide Band Gap Perovskites with Improved Stability to Photoinduced Phase Segregation. *ACS Energy Lett.* **2018**, *3* (2), 428–435. https://doi.org/10.1021/acsenergylett.7b01255.

(10)   Prasanna, R.; Gold-Parker, A.; Leijtens, T.; Conings, B.; Babayigit, A.; Boyen, H. G.; Toney, M. F.; McGehee, M. D. Band Gap Tuning via Lattice Contraction and Octahedral Tilting in Perovskite Materials for Photovoltaics. *J. Am. Chem. Soc.* **2017**, *139* (32), 11117–11124. https://doi.org/10.1021/jacs.7b04981.

(11)   Hoke, E. T.; Slotcavage, D. J.; Dohner, E. R.; Bowring, A. R.; Karunadasa, H. I.; McGehee, M. D. Reversible Photo-Induced Trap Formation in Mixed-Halide Hybrid Perovskites for Photovoltaics. *Chem. Sci.* **2015**, *6* (1), 613–617. https://doi.org/10.1039/c4sc03141e.

(12)   Al-Ashouri, A.; Köhnen, E.; Li, B.; Magomedov, A.; Hempel, H.; Caprioglio, P.; Márquez,

J. A.; Vilches, A. B. M.; Kasparavicius, E.; Smith, J. A.; Phung, N.; Menzel, D.; Grischek, M.; Kegelmann, L.; Skroblin, D.; Gollwitzer, C.; Malinauskas, T.; Jošt, M.; Matič, G.; Rech, B.; Schlatmann, R.; Topič, M.; Korte, L.; Abate, A.; Stannowski, B.; Neher, D.; Stolterfoht, M.; Unold, T.; Getautis, V.; Albrecht, S. Monolithic Perovskite/Silicon Tandem Solar Cell with >29% Efficiency by Enhanced Hole Extraction. *Science (80-.).* **2020**, *370* (6522), 1300–1309. https://doi.org/10.1126/science.abd4016.

(13)   Dunlap-Shohl, W. A.; Zhou, Y.; Padture, N. P.; Mitzi, D. B. Synthetic Approaches for Halide Perovskite Thin Films. *Chem. Rev.* **2019**, *119* (5), 3193–3295. https://doi.org/10.1021/acs.chemrev.8b00318.

(14)   Li, Z.; Klein, T. R.; Kim, D. H.; Yang, M.; Berry, J. J.; Van Hest, M. F. A. M.; Zhu, K. Scalable Fabrication of Perovskite Solar Cells. *Nat. Rev. Mater.* **2018**, *3*, 1–20. https://doi.org/10.1038/natrevmats.2018.17.

(15)   Brinkmann, K. O.; He, J.; Schubert, F.; Malerczyk, J.; Kreusel, C.; Van Gen Hassend, F.; Weber, S.; Song, J.; Qu, J.; Riedl, T. Extremely Robust Gas-Quenching Deposition of Halide Perovskites on Top of Hydrophobic Hole Transport Materials for Inverted (p-i-n) Solar Cells by Targeting the Precursor Wetting Issue. *ACS Appl. Mater. Interfaces* **2019**, *11* (43), 40172–40179. https://doi.org/10.1021/acsami.9b15867.

(16)   Dai, X.; Deng, Y.; Van Brackle, C. H.; Huang, J. Meniscus Fabrication of Halide Perovskite Thin Films at High Throughput for Large Area and Low-Cost Solar Panels. *Int. J. Extrem. Manuf.* **2019**, *1* (2), 022004. https://doi.org/10.1088/2631-7990/ab263e.

(17)   Arain, Z.; Liu, C.; Yang, Y.; Mateen, M.; Ren, Y.; Ding, Y.; Liu, X.; Ali, Z.; Kumar, M.; Dai, S. Elucidating the Dynamics of Solvent Engineering for Perovskite Solar Cells. *Sci.*

China Mater. **2019**, *62* (2), 161–172. https://doi.org/10.1007/s40843-018-9336-1.

(18)   Conings, B.; Babayigit, A.; Klug, M. T.; Bai, S.; Gauquelin, N.; Sakai, N.; Wang, J. T. W.; Verbeeck, J.; Boyen, H. G.; Snaith, H. J. A Universal Deposition Protocol for Planar Heterojunction Solar Cells with High Efficiency Based on Hybrid Lead Halide Perovskite Families. *Adv. Mater.* **2016**, *28* (48), 10701–10709. https://doi.org/10.1002/adma.201603747.

(19)   Babayigit, A.; D'Haen, J.; Boyen, H. G.; Conings, B. Gas Quenching for Perovskite Thin Film Deposition. *Joule* **2018**, *2* (7), 1205–1209. https://doi.org/10.1016/j.joule.2018.06.009.

(20)   Saliba, M.; Matsui, T.; Seo, J. Y.; Domanski, K.; Correa-Baena, J. P.; Nazeeruddin, M. K.; Zakeeruddin, S. M.; Tress, W.; Abate, A.; Hagfeldt, A.; Grätzel, M. Cesium-Containing Triple Cation Perovskite Solar Cells: Improved Stability, Reproducibility and High Efficiency. *Energy Environ. Sci.* **2016**, *9* (6), 1989–1997. https://doi.org/10.1039/c5ee03874j.

(21)   Stolterfoht, M.; Grischek, M.; Caprioglio, P.; Wolff, C. M.; Gutierrez-Partida, E.; Peña-Camargo, F.; Rothhardt, D.; Zhang, S.; Raoufi, M.; Wolansky, J.; Abdi-Jalebi, M.; Stranks, S. D.; Albrecht, S.; Kirchartz, T.; Neher, D. How To Quantify the Efficiency Potential of Neat Perovskite Films: Perovskite Semiconductors with an Implied Efficiency Exceeding 28%. *Adv. Mater.* **2020**, *32* (17). https://doi.org/10.1002/adma.202000080.

(22)   Krückemeier, L.; Rau, U.; Stolterfoht, M.; Kirchartz, T. How to Report Record Open-Circuit Voltages in Lead-Halide Perovskite Solar Cells. *Adv. Energy Mater.* **2020**, *10* (1). https://doi.org/10.1002/aenm.201902573.

(23)   Jiang, Q.; Zhao, Y.; Zhang, X.; Yang, X.; Chen, Y.; Chu, Z.; Ye, Q.; Li, X.; Yin, Z.; You, J. Surface Passivation of Perovskite Film for Efficient Solar Cells. *Nat. Photonics* **2019**. https://doi.org/10.1038/s41566-019-0398-2.

(24)   Polman, A.; Knight, M.; Garnett, E. C.; Ehrler, B.; Sinke, W. C. Photovoltaic Materials: Present Efficiencies and Future Challenges. *Science (80-.).* **2016**, *352* (6283). https://doi.org/10.1126/science.aad4424.

(25)   Zhang, H.; Lv, Y.; Wang, J.; Ma, H.; Sun, Z.; Huang, W. Influence of Cl Incorporation in Perovskite Precursor on the Crystal Growth and Storage Stability of Perovskite Solar Cells. *ACS Appl. Mater. Interfaces* **2019**, *11* (6), 6022–6030. https://doi.org/10.1021/acsami.8b19390.

(26)   Hu, Y.; Aygüler, M. F.; Petrus, M. L.; Bein, T.; Docampo, P. Impact of Rubidium and Cesium Cations on the Moisture Stability of Multiple-Cation Mixed-Halide Perovskites. *ACS Energy Lett.* **2017**, *2* (10), 2212–2218. https://doi.org/10.1021/acsenergylett.7b00731.

(27)   Tan, H.; Che, F.; Wei, M.; Zhao, Y.; Saidaminov, M. I.; Todorović, P.; Broberg, D.; Walters, G.; Tan, F.; Zhuang, T.; Sun, B.; Liang, Z.; Yuan, H.; Fron, E.; Kim, J.; Yang, Z.; Voznyy, O.; Asta, M.; Sargent, E. H. Dipolar Cations Confer Defect Tolerance in Wide-Bandgap Metal Halide Perovskites. *Nat. Commun.* **2018**, *9* (1). https://doi.org/10.1038/s41467-018-05531-8.